Synthesis of an S_T = 7 [Mn$_3$] Mixed-Valence Complex Based on 1,3-Propanediol Ligand Derivatives and Its One-Dimensional Assemblies

Jian Huang,[†] Gang Wu,*,[†] Jiaquan Bai,[†] Yuan Jiang,[†] Guanghua Li,[†] Shilun Qiu,*,[†] and Rodolphe Clérac*,[‡,§]

[†]State Key Laboratory of Inorganic Synthesis & Preparative Chemistry, Jilin University, 2699 Qianjin Street, 130012 Changchun, P. R. China

[‡]CNRS, CRPP, UPR 8641, F-33600 Pessac, France

[§]University of Bordeaux, CRPP, UPR 8641, F-33600 Pessac, France

Ⓢ *Supporting Information*

ABSTRACT: Controlled organization of high-spin complexes and single-molecule magnets is a great challenge in molecular magnetism in order to study the effect of the intercomplex magnetic interactions on the intrinsic properties of a given magnetic object. In this work, a new S_T = 7 trinuclear mixed-valence Mn complex, $[Mn^{III}Mn^{II}_2(L_A)_2(Br)_4(CH_3OH)_6]\cdot Br\cdot(CH_3OH)_{1.5}\cdot(H_2O)_{0.5}$ (**1**), is reported using a pyridinium-functionalized 1,3-propanediol ligand (H_2L_ABr = 1-(3-bromo-2,2-bis(hydroxymethyl)propyl)pyridinium bromide). Using

azido anions as bridging ligands and different pyridinium-functionalized 1,3-propanediol ligands (H_2L_BBr = 1-(3-bromo-2,2-bis(hydroxymethyl)propyl)-4-picolinium bromide; H_2L_CBr = 1-(3-bromo-2,2-bis(hydroxymethyl)propyl)-3,5-lutidinium bromide), the linear $[Mn^{III}Mn^{II}_2L_2X_4]^+$ building block has been assembled into one-dimensional coordination networks: $[Mn^{III}Mn^{II}_2(L_A)_2(Br)_4(CH_3OH)_4(N_3)]\cdot((C_2H_5)_2O)_{1.25}$ (**2∞**), $[Mn^{III}Mn^{II}_2(L_B)_2(Br)_4(C_2H_5OH)(CH_3OH)(H_2O)_2(N_3)]\cdot(H_2O)_{0.25}$ (**3∞**), and $[Mn^{III}Mn^{II}_2(L_C)_2(Cl)_{3.8}(Br)_{0.2}(C_2H_5OH)_3(CH_3OH)(N_3)]$ (**4∞**). The syntheses, characterization, crystal structures, and magnetic properties of these new [Mn$_3$]-based materials are reported.
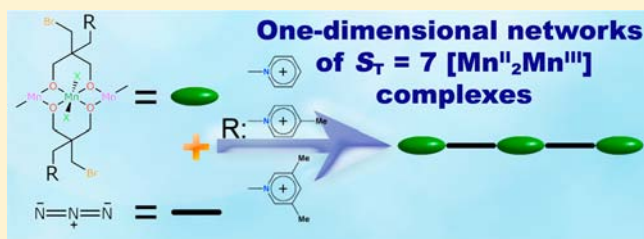
■ INTRODUCTION

Polynuclear Mn complexes have been of great interest for their relevance to various research areas such as bioinorganic chemistry[1] and molecular nanoscience.[2] A representative metalloenzyme example in bioinorganic chemistry is the oxygen-evolving complex (OEC) in photosystem II (PS II) of green plants that contains a Mn_4CaO_x active site.[1a,b,3] In the field of molecular magnetism, polynuclear Mn complexes have attracted much attention since the discovery of the single-molecule magnets (SMMs) at the beginning of the 1990s. These complexes are molecular objects which possess a significant energy barrier to magnetization relaxation and consequently function as nanoscale magnets.[4] Interestingly, in 2002, Christou and Wernsdorfer showed that weak supramolecular interactions between SMMs can modulate their intrinsic thermodynamic and quantum properties.[5] Therefore, it becomes natural to design coordination objects or networks based on SMM or high-spin building blocks to probe the influence of significant magnetic interactions on the SMM slow dynamics and also to explore novel magnetic properties at the frontier between SMMs and classical ordered magnets.[6] In both cases, the chemical and physical stability of the magnetic synthons during the self-assembly processes is the key factor to obtain new magnetic materials. In contrast with polyoxometallate systems, metal–organic frameworks, and metal phosphate networks,[7−9] current advances in SMM-based or high-spin complex-based materials is restricted to a very limited number of building blocks.[10,11] This relatively recent area of research is currently a very active topic in the field of molecular magnetism motivating many groups worldwide to design coordination aggregates or extended networks based on new SMM or high-spin molecule units.[6o]

1,3-Propanediol ligand derivatives have been used to synthesize a broad variety of Mn aggregates with aesthetically pleasing structures and interesting magnetic properties.[12] Among these complexes, mixed-valence $[Mn^{III}_6Mn^{II}_4]$ and $[Mn^{III}_{11}Mn^{II}_6]$ species, which possess high-spin ground states (S_T = 22 and 37 respectively), have been used as magnetic synthons to build extended coordination networks with unusual slow magnetization dynamics and long-range magnetic orders.[6m,12g−i] As a natural expansion of these works, a new series of coordination materials based on a linear S_T = 7 $[Mn^{II}_2Mn^{III}]$ building block has been obtained. Our synthetic strategy employs pyridinium-functionalized 1,3-diol chelating ligands to form a robust $[Mn^{III}Mn^{II}_2]$ core and azide anions as linkers to construct one-dimensional $[Mn^{II}_2Mn^{III}]$-based magnetic networks.

■ EXPERIMENTAL SECTION

Synthesis. All chemicals were obtained commercially without further purification; organic synthesis took place under argon atmosphere, while other manipulations were at ambient conditions. *Caution! Although no such tendency was observed during the present work, azide salts are potentially explosive and should be handled with care and in small quantities.*

Ligands Preparation. All ligands were prepared through a new method adapted from the literature.[13] 2,2-Bis(bromomethyl)-1,3-propanediol (20 mmol) and the corresponding pyridine derivatives (pyridine, 4-picoline, and 3,5-lutidine, 30 mmol) were dissolved in *N,N'*-dimethylformamide (DMF, 10 mL). The mixture was heated to 130 °C for 18 h while thoroughly stirring. After cooling to room temperature, the resulting dark solution was poured into diethyl ether. Light-colored precipitates formed immediately. The suspension was left undisturbed for ca. 3 h to settle the crude product.

1-(3-Bromo-2,2-bis(hydroxymethyl)propyl)pyridinium Bromide (H$_2$L$_A$Br). The crude product was pure enough for coordination reactions, collected in 55% yield as a white powder by suction filtration, and washed with ethylacetate. Anal. Calcd for H$_2$L$_A$Br (C$_{10}$H$_{15}$NO$_2$Br$_2$): C, 35.2; H, 4.43; N, 4.11. Found: C, 35.8; H, 4.88; N, 4.38. FTIR: (KBr pellets, cm^{-1}): $\bar{\nu}$ = 3270(s), 3056(m), 2881(w), 2805(w), 1630(s), 1487(s), 1437(m), 1338(m), 1253(m), 1178(m), 1068(m), 1016(s), 875(m), 755(m), 688(m), 617(m), 497(w). ^{1}H NMR (300 MHz, DMSO-d_6), δ = 3.26−3.45 (t, 6H, *J* = 12 Hz, CH$_2$), 4.16−4.45 (m, 2H, OH), 4.5 4.62 (s, 2H, py$^+$−CH$_2$), 7.96−8.85 (m, 5H, py).

1-(3-Bromo-2,2-bis(hydroxymethyl)propyl)-4-picolinium Bromide (H$_2$L$_B$Br). Crude product was pure enough for the next reactions and collected as light orange solids in 66% yield by suction filtration and washed by ethylacetate. Anal. Calcd for H$_2$L$_B$Br (C$_{11}$H$_{17}$NO$_2$Br$_2$): C, 37.2; H, 4.83; N, 3.94. Found: C, 37.7; H, 4.92; N, 4.88. FTIR: (KBr pellets, cm^{-1}): $\bar{\nu}$ = 3303(s), 3060(w), 2929(w), 1641(s), 1467(m), 1423(m), 1319(m), 1245(m), 1180(m), 1056(m), 1006(s), 879(w), 829(m), 782(m), 653(w), 604(m), 568(m), 485(m). ^{1}H NMR (300 MHz, DMSO-d_6), δ = 3.29 (s, 2H, Br−CH$_2$), 3.40 (s, 4H, CH$_2$), 4.48 (s, 2H, py$^+$−CH$_2$), 4.64 (s, 3H, py−CH$_3$), 7.72 − 8.53 (d, 4H, *J* = 7 Hz, py).

1-(3-Bromo-2,2-bis(hydroxymethyl)propyl)-3,5-lutidinium Bromide (H$_2$L$_C$Br). The crude liquid product was separated and recrystallized in MeCN or EtOH to afford white to colorless prism crystals in 48% yield. Anal. Calcd for H$_2$L$_C$Br (C$_{12}$H$_{19}$NO$_2$Br$_2$): C, 39.1; H, 5.19; N, 3.79. Found: C, 39.6; H, 5.58; N, 3.90. FTIR: (KBr pellets, cm^{-1}): $\bar{\nu}$ = 3261(s), 3070(w), 2883(w), 2805(w), 1637(m), 1492(m), 1382(m), 1305(m), 1054(s), 871(m), 773(w), 713(w), 671(m), 620(m), 455(w). ^{1}H NMR (300 MHz, DMSO-d_6), δ = 2.37 (m, 6H, CH$_2$), 3.30 (d, 2H, py$^+$−CH$_2$), 3.35 (d, 2H, OH), 4.40 − 4.45 (m, 6H, py−CH$_3$), 8.14 (s, 1H, py), 8.36 (s, 2H, py).

[Mn^{III}Mn^{II}$_2$(L$_A$)$_2$Br$_4$(CH$_3$OH)$_6$]Br·1.5CH$_3$OH·0.5 H$_2$O (1). A 40% methanolic solution of tetra-*n*-butylammonium hydroxide (0.16 mL) was added dropwise with stirring with a 10 mL methanol solution of MnBr$_2$·4H$_2$O (0.17 g, 0.6 mmol) and H$_2$L$_A$Br (0.14 g, 0.4 mmol). A reddish orange solution formed after further 2 h stirring. This solution was filtered and layered by a diethyl ether and hexane mixture (1:1). Orange block crystals were isolated in 2 weeks in 52% yield (based on Mn). Anal. Calcd for [Mn$_3$(L$_A$)$_2$Br$_4$(CH$_3$OH)$_6$]Br·1.5CH$_3$OH· 0.5H$_2$O (1) (C$_{27.5}$H$_{57}$O$_{12}$N$_2$Br$_7$Mn$_3$): C, 24.80; H, 4.31; N, 2.10. Found: C, 23.90; H, 4.92; N, 1.90. Selected IR data (KBr pellet): $\bar{\nu}$ = 3347(s), 3056(m), 2859(m), 1631(s), 1490(s), 1455(m), 1405(w), 1371(w), 1354(w), 1216(w), 1178(m), 1141(m), 1079(s), 958(w), 775(m), 750(m), 690(s), 638(m), 586(s), 530(m).

[Mn^{III}Mn^{II}$_2$(L$_A$)$_2$(Br)$_4$(CH$_3$OH)$_4$(N$_3$)]·((C$_2$H$_5$)$_2$O)$_{1.25}$ (2∞). ****Keeping a vigorous stirring, NaN$_3$ (0.02 g, 0.3 mmol) was added to a methanol (2 mL) and dichloromethane (4 mL) solution containing MnBr$_2$·4H$_2$O (0.12 g, 0.4 mmol), and H$_2$L$_A$Br (0.07 g, 0.3 mmol). After 15 min, tetra-*n*-butylammonium bromide (0.8 g) was added and the solution was stirred for further 2 h. The resulting orange/red solution was left undisturbed in diethylether atmosphere at room temperature to obtain yellow/red crystals in one week with 33% yield (based on Mn). Anal. Calcd for [Mn$_3$(L$_A$)$_2$(Br)$_4$(CH$_3$OH)$_4$(N$_3$)]·

((C$_2$H$_5$)$_2$O)$_{1.25}$ (2)∞ (C$_{29}$H$_{54.5}$O$_{9.25}$N$_5$Br$_6$Mn$_3$): C, 27.52; H, 4.34; N, 5.53. Found: C, 27.31; H, 4.12; N, 6.09. Selected IR data (KBr pellet): $\bar{\nu}$ = 3332(s), 3080(m), 2900(m), 2080(s), 1630(m), 1487(s), 1177(w), 1103(m), 1076(s), 1055(s), 796(w), 758(w), 688(m), 623(m), 611(s), 536(m).

[Mn^{III}Mn^{II}$_2$(L$_B$)$_2$(Br)$_4$(C$_2$H$_5$OH)(CH$_3$OH)(H$_2$O)$_2$(N$_3$)]·0.25H$_2$O (3∞). Solid NaN$_3$ (0.02 g, 0.3 mmol) was added to a methanol (2 mL) and ethanol (4 mL) mixture of MnBr$_2$·4H$_2$O (0.12 g, 0.4 mmol) and H$_2$L$_B$Br (0.07 g, 0.2 mmol). The resulting red solution was filtered after stirring about 1 h and then layered with a diethyl ether/hexane mixture (1:1). Red prism crystals formed after 7 days in 46% yield (based on Mn). Anal. Calcd for [Mn$_3$(L$_B$)$_2$(Br)$_4$(C$_2$H$_5$OH)- (CH$_3$OH)(H$_2$O)$_2$(N$_3$)]·0.25H$_2$O (3)∞ (C$_{25}$H$_{44.5}$O$_{8.25}$N$_5$Br$_6$Mn$_3$): C, 25.20; H, 3.76; N, 5.88. Found: C, 24.72; H, 4.03; N, 5.98. Selected IR data (KBr pellet): $\bar{\nu}$ = 3367(s), 2856(m), 2096(s), 1639(s), 1513(m), 1473(m), 1390(w), 1315(w), 1176(m), 1108(s), 1064(s), 877(w), 827(m), 659(m), 595(s), 557(m), 499(m).

[Mn^{III}Mn^{II}$_2$(L$_C$)$_2$(Cl)$_{3.8}$(Br)$_{0.2}$(C$_2$H$_5$OH)$_3$(CH$_3$OH)(N$_3$)] (4∞). To a mixture of methanol (5 mL) and ethanol (7 mL) containing MnCl$_2$· 4H$_2$O (0.12 g, 0.6 mmol) and H$_2$L$_C$Br (0.15 g, 0.4 mmol) was added solid NaN$_3$ (0.04 g, 0.6 mmol). After 1 h stirring, the resulting orange to red solution was filtered and the filtrate was left undisturbed for slow evaporation. Red block crystals were formed within 7 days in 72% yield (based on Mn). Anal. Calcd for [Mn$_3$(L$_C$)$_2$(Cl)$_{3.8}$(Br)$_{0.2}$(C$_2$H$_5$OH)$_3$(CH$_3$OH)(N$_3$)] (4∞) (C$_{31}$H$_{56}$O$_8$N$_5$Cl$_{3.8}$Br$_{2.2}$Mn$_3$): C, 33.78; H, 5.12; N, 6.35. Found: C, 33.17; H, 6.20; N, 6.61. Selected IR data (KBr pellet): $\bar{\nu}$ = 3380(s), 2076(s), 1625(m), 1494(m), 1448(w), 1390(m), 1303(w), 1186(w), 1122(m), 1070(s), 879(m), 835(w), 671(m), 615(m), 584(s). X-ray photoelectron spectroscopy (XPS) measurement confirmed the coexistence of Br and Cl in 4 (Figure S8, Supporting Information).

X-ray Data Collection and Structure Refinement. Single-crystal structure determinations were carried out on a Siemens SMART CCD diffractometer equipped with graphite-monochromated Mo Kα radiation (λ = 0.71073 Å) at 170 ± 2 K. Data processing was accomplished with the SAINT[14a] processing program. Structures were solved by direct methods and refined with the full-matrix least-squares technique using the program SHELXTL-97.[14b] Anisotropic thermal parameters were assigned to all non-hydrogen atoms.

Magnetic Measurements. Magnetic susceptibility measurements were carried out on a Quantum Design SQUID magnetometer MPMS-XL housed at the Centre de Recherche Paul Pascal (CRPP). This magnetometer operates between 1.8 and 400 K for applied dc fields ranging from −70 to 70 kOe. Measurements were performed on polycrystalline samples of 1 (9.14 mg), 2∞ (20.37 mg), 3∞ (6.63 mg), and 4∞ (40.20 mg) loaded into a polyethylene bag (3 × 0.5 × 0.02 cm). The purity of all four complexes was confirmed by powder X-ray diffraction (pXRD) (Figures S4−S7, Supporting Information). The ac susceptibility measurements were measured with an oscillating ac field of 3 Oe with ac frequencies from 1 to 1500 Hz. For 1, 3∞, and 4∞, these ac susceptibility measurements below 15 K show a complete absence of out-phase signal above 1.8 K. An *M* vs *H* measurement was performed at 100 K to confirm the absence of ferromagnetic impurities. Experimental data were corrected for the sample holder and the diamagnetic contribution of the sample.
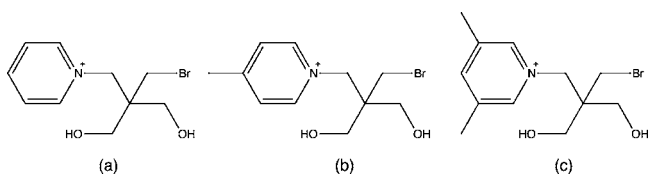
Other Physical Characterizations. Elemental analysis (C, H, and N) was carried out on a Perkin-Elmer 2400 Elemental Analysis. IR spectra were recorded in the range 400−4000 cm^{-1} on a Bruker IFS 66v/S IR spectrometer using KBr pellets. ^{1}H NMR spectra were recorded in deuterated DMSO with a 300 MHz Mercury Varian-300 NMR spectrometer. Powder X-ray diffraction (pXRD) were recorded with a Rigaku D/Max 2550 XRD diffractometer. X-ray photoelectron spectroscopy (XPS) were recorded with a Thermo Scientific ESCALAB250 Xi XPS spectrometer.

■ RESULTS AND DISCUSSION

Synthesis. 1,3-Propanediol derivatives, sometimes associated with carboxylate or nitrogen donor molecules as coligands, led to a variety of Mn aggregates[12] including high-spin [Mn$_{10}$]

and [Mn$_{17}$] complexes. Thanks to the versatile coordination abilities of these molecular species, new magnetic architectures and coordination networks of [Mn$_{10}$] and [Mn$_{17}$] units have been obtained.[8,12g−i] Along this line of research, we dedicated our work to a rational and methodical modification of the 1,3-diol ligand uncoordinating groups to investigate its impact on the final manganese aggregate and crystal packing. The choice of ligand functionalization should obviously direct the synthesis of new complexes with different nuclearity, geometry, oxidation state, intra- and intercomplex magnetic interactions, and thus spin-ground state. In this frame, the coordination chemistry of cationic 1,3-diol ligands such as H$_2$L$_A^+$, H$_2$L$_B^+$, and H$_2$L$_C^+$ (shown in Scheme 1) with manganese salts has been explored.

These 1,3-diol pyridinium-containing ligands were designed and synthesized through simple reactions of 2,2-bis-(bromomethyl)-1,3-propanediol with corresponding pyridine derivatives in DMF (see Experimental Section). Reaction of H$_2$L$_A$Br with MnBr$_2$ in basic methanol resulted in complex **1** in 52% yield. After a close investigation of the crystal structure of **1** (vide infra), it appears that peripheral Mn^{II} ions possessed available coordination sites and therefore could be potentially used to build extended coordination networks. As expected, introducing an appropriate bridging ligand, such as azido anions, one-dimensional networks were obtained based on the [Mn$_3$] building block with the H$_2$L$_A^+$, H$_2$L$_B^+$, and H$_2$L$_C^+$ ligands (Scheme 1). The different functionalizations of the 1,3-diol ligands allowed us to systematically investigate their effect on the final [Mn$_3$] aggregate, its crystal packing, and eventually the magnetic properties.

Structure Description. Crystal structures of **1**, **2∞**, **3∞**, and **4∞**, shown in Figures 1−4, were studied by single-crystal X-ray diffraction (see Experimental Section). These four complexes crystallize in monoclinic $P2_1/c$, $P2_1/n$, and $C2/c$ space groups for **1**, **2∞**, and **4∞**, respectively, and in the P-1 triclinic space group for **3∞**. In all these complexes a trinuclear
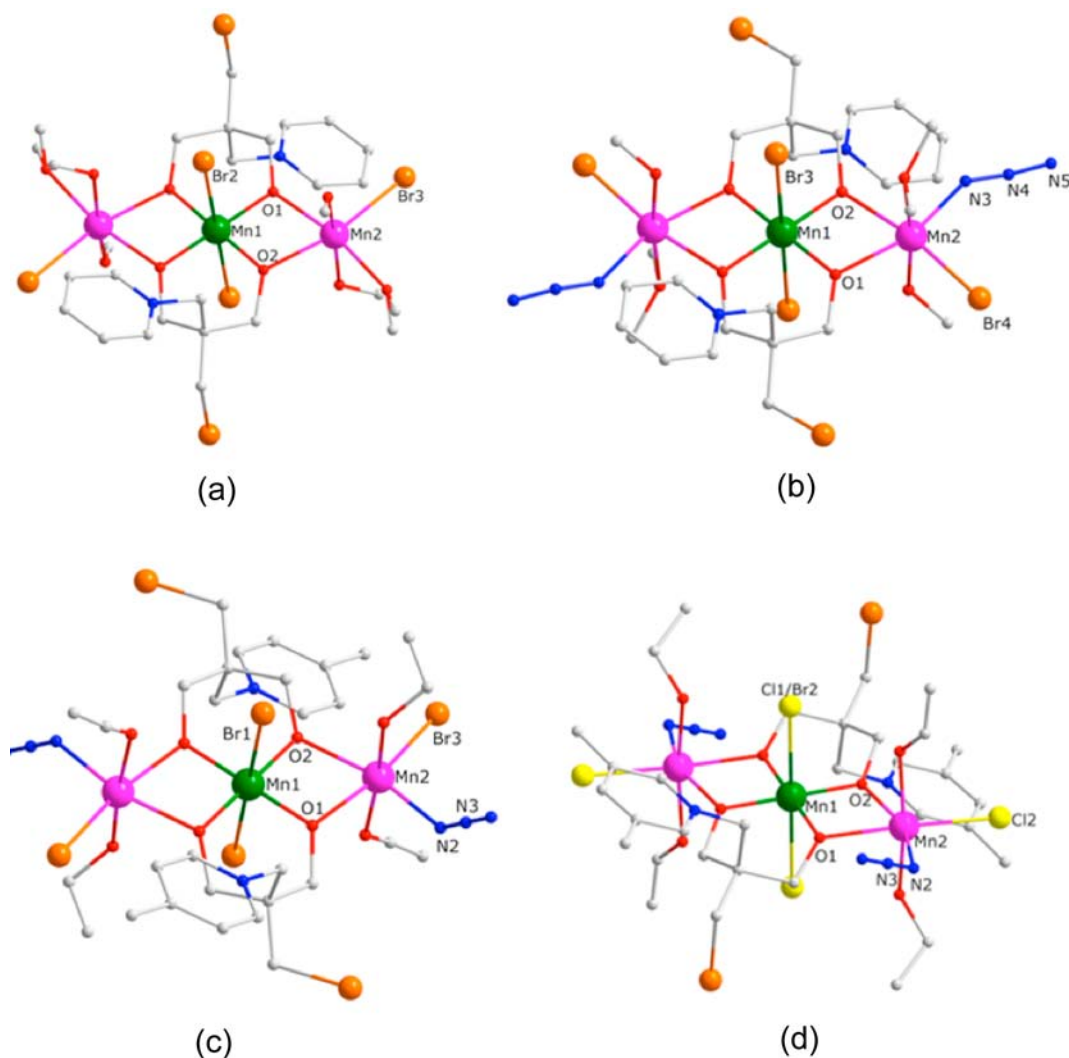
Scheme 1. Designed Cationic Ligands: (a) H$_2$L$_A^+$, (b) H$_2$L$_B^+$, and (c) H$_2$L$_C^+$

Figure 1. View of the molecular structure of the [Mn^{II}$_2$Mn^{III}] unit in (a) **1**, (b) **2∞**, (c) **3∞**, and (d) **4∞** with atom-labeling scheme: Mn^{III}, green; Mn^{II}, pink; Cl, yellow; Br, orange; N, blue; O, red; C, gray. All hydrogen atoms, counterions, and guest molecules are omitted for clarity.
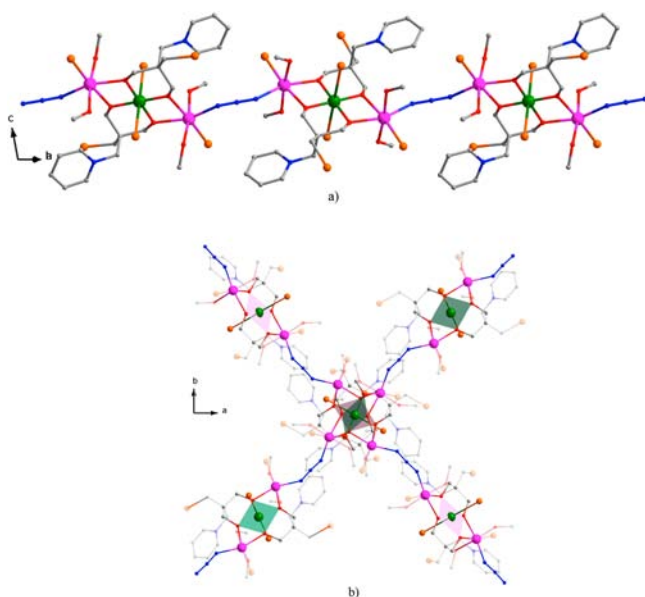
Figure 2. Views of the one-dimensional coordination network in **2∞** emphasizing (a) the azido-bridged chain of [Mn$^{II}_2$Mn^{III}] units and (b) the two different chain orientations in the crystal packing: Mn^{III}, green; Mn^{II}, pink; Br, orange; N, blue; O, red; C, gray. All hydrogen atoms and guest molecules are omitted for clarity.

Figure 3. Views of the one-dimensional coordination network in **3∞** emphasizing (a) the azido-bridged chain of [Mn$^{II}_2$Mn^{III}] units and (b) the parallel chain orientation in the crystal packing: Mn^{III}, green; Mn^{II}, pink; Br, orange; N, blue; O, red; C, gray. All hydrogen atoms and guest molecules are omitted for clarity.
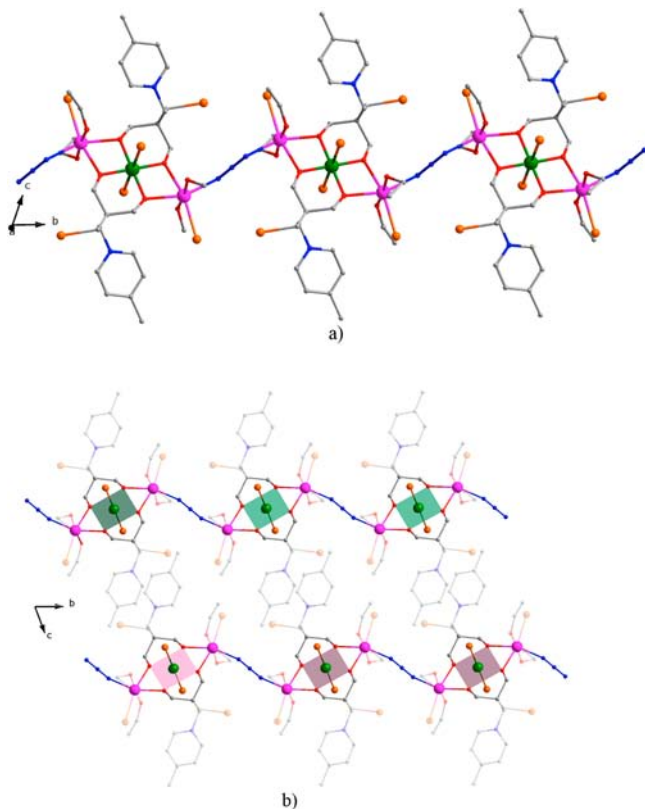
centrosymmetrical [Mn(II)−(μ-O)$_2$−Mn(III)−(μ-O*)$_2$−Mn*(II)] complex, assembled by two fully deprotonated monoanionic L$^-$ ligand, is observed as an isolated species in
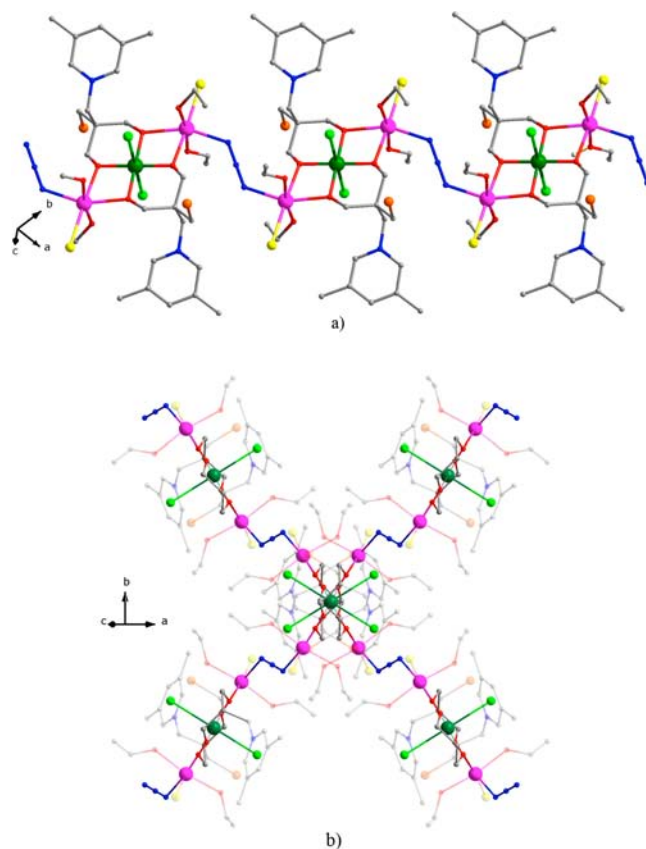

Figure 4. Views of the one-dimensional coordination network in **4∞** emphasizing (a) the azido-bridged chain of [Mn$^{II}_2$Mn^{III}] units and (b) the two chain orientations in the crystal packing: Mn^{III}, green; Mn^{II}, pink; Br, orange; Cl, yellow; disordered Br/Cl, light green; N, blue; O, red; C, gray. All hydrogen atoms are omitted for clarity.

1 or as the repeating unit of a one-dimensional azido-bridged coordination network in **2∞**, **3∞**, and **4∞**. Crystallographic details on these complexes are summarized in Table 1, and the main bond distances and angles are given in Tables S1−S4, Supporting Information.

In **1**, the central Mn1 ion adopts a distorted octahedral coordination sphere with four oxygen atoms of two fully deprotonated L$_A^-$ ligands in equatorial positions (the average Mn1−O bond distance being 1.882(4) Å) and two axially coordinated bromide anions (Figure 1a). The strong Jahn−Teller distortion observed along the Br2−Mn1−Br2* axis, with extremely long Mn1−Br2 bonds around 3.050 Å, indicates without ambiguity a +III oxidation state for the central Mn site. The two peripheral Mn2 ions are hexacoordinated with three terminal methanol molecules, one Br$^-$, and two μ-oxygen atoms from two L$_A^-$ ligands that bridge the two Mn sites with Mn1−O1−Mn2 and Mn1−O2−Mn2 angles of 102.39(18)° and 103.44(18)°, respectively, and a Mn1−Mn2 distance of 3.1902(9) Å. While the average Mn2−O bond distance is 2.209(5) Å, the Mn−Br one is as expected slightly longer at 2.5897(11) Å. The coordination sphere of the Mn2 site is fully compatible with an +II oxidation state as also confirmed by bond valence calculations and charge balance (Table S5, Supporting Information). The charge of the cationic [Mn^{III}Mn$^{II}_2$(L$_A$)$_2$Br$_4$]$^+$ core is balanced in the crystal structure by a single Br$^-$ ion that is implicated in multiple C−H···Br interactions between [Mn$_3$] units.

Table 1. Crystallographic Data of Complexes 1, 2∞, 3∞, and 4∞

	1	2∞	3∞	4∞
empirical formula	$C_{27.5}H_{57}N_2O_{12}Br_7Mn_3$	$C_{29}H_{54.5}N_5O_{9.25}Br_6Mn_3$	$C_{25}H_{44.5}N_5O_{8.25}Br_6Mn_3$	$C_{31}H_{56}N_5O_8Cl_{3.8}Br_{2.2}Mn_3$
fw, g mol^{-1}	1331.871	1265.56	1191.376	1102.14
cryst syst	monoclinic	monoclinic	triclinic	monoclinic
space group	$P2_1/c$	$P2_1/n$	$P\text{-}1$	$C2/c$
a (Å)	13.2315(7)	16.342(8)	9.1753(9)	14.037(4)
b (Å)	12.3924(7)	16.809(8)	10.9771(1)	14.131(4)
c (Å)	14.3405(8)	19.303(9)	12.3416(1)	24.141(6)
α (deg)	90	90	69.791(2)	90
β (deg)	107.063(1)	104.780(7)	83.716(2)	101.963(5)
γ (deg)	90	90	88.918(2)	90
V (Å^3)	2247.9(2)	5127(4)	1159.3(2)	4785(2)
Z	2	4	1	4
D (calcd, g cm^{-3})	1.955	1.640	1.709	1.563
μ (mm^{-1})	7.102	5.448	6.017	2.936
F (000)	1294	2490	580	2230
2θ range for data collection (deg)	2.22−25.12	1.77−25.14	1.77−26.07	1.72−28.32
index ranges	$-15 \leq h \leq 15$	$-18 \leq h \leq 19$	$-11 \leq h \leq 11$	$-18 \leq h \leq 17$
	$-14 \leq k \leq 14$	$-11 \leq k \leq 19$	$-13 \leq k \leq 13$	$-17 \leq k \leq 18$
	$-10 \leq l \leq 17$	$-22 \leq l \leq 23$	$-15 \leq l \leq 13$	$-32 \leq l \leq 30$
no. of measd reflns	11 053	24362	6293	16 424
no. of independent reflns	3951	8880	4440	5749
R_{int}	0.0254	0.0707	0.0233	0.0564
refined params	232	520	256	247
obsd reflns with $I \geq 2\sigma(I)$	3951	8880	4440	5749
goodness-of-fit on F^2, S	1.058	0.987	0.863	1.061
$R_1{}^a$, $wR_2{}^b$ [$I \geq 2\sigma(I)$]	0.0513, 0.1398	0.0553, 0.1519	0.0557, 0.1531	0.0991, 0.2693
$R_1{}^a$, $wR_2{}^b$ [all data]	0.0676, 0.150	0.0908, 0.1674	0.0854, 0.1770	0.1456, 0.2951
max, min electron density (e Å^{-3})	1.111, −1.593	1.223, −0.816	1.023, −1.235	1.486, −0.983

$^a R_1 = [\Sigma||F_0| - |F_C||/\Sigma|F_0|]$. $^b wR_2 = [\Sigma w(F_0{}^2 - F_C{}^2)^2/\Sigma wF_0{}^4]^{1/2}$.

[Mn₃] complexes with linear [Mn^{II}−Mn^{III}−Mn^{II}] topology have been reported in various ligand systems.[15] However, in most cases, the bulky chelating ligands (for example, macrocyclic-type ligand, 2,2′-bipyridine, and N,N,N′,N′-tetrakis(2-hydroxyethyl)ethylenediamine) block all coordination sites on Mn^{II} ions and thus prevent further assembly of such fragments. Interestingly, in 1 the two peripheral Mn^{II} ions remain 'open' for further coordination with the possibility to replace labile coordinating groups such as methanol molecules or even bromide anions. In order to substitute these potential leaving groups, synthesis of 1 was performed in the presence of bridging ligands that could lead to coordination networks of [Mn^{III}Mn$^{II}_2$L$_2$X$_4$]$^+$ units (X being Br or Cl anions).

When azide anions were used, one-dimensional assemblies of azido-bridged [Mn^{III}Mn$^{II}_2$L$_2$X$_4$]$^+$ moieties were obtained reproducibly with the three different types of 1,3-diol pyridinium-containing ligands shown in Scheme 1. In these complexes, 2∞, 3∞, and 4∞, the [Mn^{III}Mn$^{II}_2$L$_2$X$_4$]$^+$ moiety remains intact (Figure 1b, 1c, and 1d) and quasi-identical, although the coordination sphere of the peripheral Mn^{II} ions has been modified by the presence of a coordinating azido ligand. It is worth mentioning that two crystallographically independent [Mn^{III}Mn$^{II}_2$(L$_A$)$_2$Br$_4$]$^+$ units are observed in 2∞ even if they exhibit a very similar geometry in terms of bond distances and angles (Tables S1−S4, Supporting Information). As observed in 1, the central Mn site of the [Mn^{III}Mn$^{II}_2$L$_2$X$_4$]$^+$ moieties displays a distorted octahedral coordination sphere with four oxygen atoms of two fully deprotonated L$^-$ ligands in equatorial positions (average Mn−O bond distances being 1.883(4), 1.878(4), and 1.890(5) Å for 2∞, 3∞, and 4∞,

respectively) and two axially coordinated halide (X) anions: bromide in 2∞ (Figure 1b) and 3∞ (Figure 1c) and disordered Cl/Br (90%/10%) anions in 4∞ (Figure 1d). A strong Jahn−Teller effect is observed along the X−Mn1/3−X* axis, with relatively long Mn−X bonds (3.120(1), 3.046(3), and 2.858(2) Å for 2∞, 3∞, and 4∞, respectively). This structural feature implies without ambiguity a +III oxidation state for the central Mn site as already observed in 1. The two peripheral Mn sites possess an octahedral coordination sphere with two terminal solvent molecules (two methanol molecules in 2∞; two disordered solvents consisting of one water, one-half methanol, and one-half ethanol molecules in 3∞; an ethanol and a disordered one-half methanol and one-half ethanol molecule in 4∞), two μ-oxygen atoms from two L$^-$ ligands, one Br$^-$ (in 2∞ and 3∞) or one Cl$^-$ (in 4∞) and one azide anion. The two oxygen atoms of the L$^-$ ligands bridge the Mn^{II} and Mn^{III} metal ions with average Mn−O−Mn angles of 102.4(2)° for 2∞, 102.88(18)° for 3∞, and 102.6(2)° for 4∞. This double μ-alkoxido bridge leads to Mn^{II}−Mn^{III} distances of 3.195(1), 3.195(1), and 3.200(1) Å for 2∞, 3∞, and 4∞, respectively. While the average Mn^{II}−O and Mn^{II}−N bond distances are 2.215(5)/2.166(6), 2.202(5)/2.152(7), and 2.207(7)/2.203(9) Å for 2∞, 3∞, and 4∞, respectively, the average Mn^{II}−X one is as expected slightly longer at 2.589(2), 2.596(1), and 2.516(2) Å, respectively. As also confirmed by bond valence calculations and charge balance, the coordination sphere of the peripheral Mn sites is fully compatible with an +II oxidation state.

While in 1 the charge of the cationic [Mn^{III}Mn$^{II}_2$L$_2$X$_4$]$^+$ complex is balanced by a single interstitial Br$^-$ ion, the anionic

11055

dx.doi.org/10.1021/ic401269p | *Inorg. Chem.* 2013, 52, 11051−11059

end-to-end bridging azido groups (with average $Mn^{II}-N-N$ angles of 145.3(6)°, 132.5(7)°, and 126.5(7)° for **2∞**, **3∞**, and **4∞** respectively) are ensuring the presence of neutral chains for the three other compounds (Figures 2, 3, and 4). Along the chain direction, the Jahn−Teller axes of the Mn^{III} sites (which defines the local easy magnetic axis) form a large angle of 84.8° between two neighboring $[Mn^{III}Mn^{II}_2(L_A)_2Br_4]^+$ units in **2∞** (Figure 2a). On the other hand, the Jahn−Teller axes are parallel to each other by symmetry along the one-dimensional network in **3∞** and **4∞** (Figures 3a and 4a). In the crystal packing the chains are running strictly parallel along the b axis in **3∞** (Figure 3b), while in **2∞** and **4∞** they are oriented in two different directions that form angles of 66.4° and 82.1°, respectively (Figures 2b and 4b). In the crystal packing of **3∞**, the chains self-assemble in the bc plane into a two-dimensional supramolecular network by cationic $\pi-\pi$ stacking through 4-picolinium rings of the L_B ligand (Scheme 1). Such cationic $\pi-\pi$ interaction is not observed in the other compounds. Therefore, this weak interaction might be the consequence of the electron-donating effect of the para methyl group that induces a larger distribution of the nitrogen positive charge on the aromatic ring. Consequently, the electronic repulsion is minimized and the $\pi-\pi$ stacking becomes possible. In **4∞**, the combined effects of the increased steric hindrance of 3,5-methyl substitution and the weaker electron-donating ability of the meta methyl groups to the positive charge might destabilize these cationic $\pi-\pi$ interactions.

Magnetic Properties. The magnetic properties of the four $[Mn^{III}Mn^{II}_2L_2X_4]^+$-based compounds have been investigated by dc and ac susceptibility measurements between 1.8 and 300 K. The temperature dependence of the dc magnetic susceptibility at 1000 Oe is reported for each compound as χT vs T plots in Figures 5 and 6.
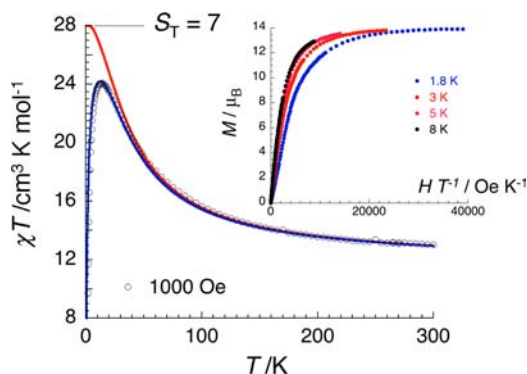

Figure 5. Temperature dependence of χT at 1000 Oe for **1**, where χ is defined as the molar magnetic susceptibility equal to M/H per mole of $[Mn^{III}Mn^{II}_2(L_A)_2Br_4]^+$ complex. Solid lines are the best fits of the experimental data with the Heisenberg trinuclear $[Mn^{II}-Mn^{III}-Mn^{II}]$ model with (blue) and without (red) intercomplex magnetic interactions treated in the mean-field approximation (see text). (Inset) M vs H/T data for **1** at the indicated temperatures, scanning at about 100−200 Oe min^{-1}.

For **1**, the χT product measured at 300 K (Figure 5) is 13.0 cm^3 K mol^{-1} that is higher than the theoretical spin-only value (11.75 cm^3 K mol^{-1}) for two Mn^{II} ($C = 4.375$ cm^3 K mol^{-1} with $g = 2$) and one Mn^{III} ($C = 3$ cm^3 K mol^{-1} with $g = 2$) magnetic centers. Upon lowering the temperature, the χT product increases gradually to a maximum of 24.1 cm^3 K mol^{-1} at 13 K, indicating the existence of dominant ferromagnetic
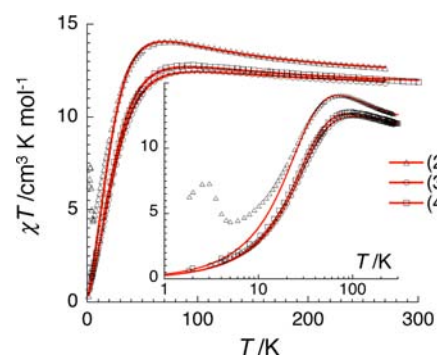

Figure 6. Temperature dependence of χT (main figure, in linear scales; inset, semilogarithm plot) at 1000 Oe for **2∞**, **3∞**, and **4∞**, where χ is defined as the molar magnetic susceptibility equal to M/H per mole of $[Mn^{III}Mn^{II}_2L_2X_4]^+$ complex. Red solid lines are the best fits of the experimental data with the Heisenberg $\cdots[Mn^{II}-Mn^{III}-Mn^{II}]\cdots$ chain model (see text).

interactions within the trinuclear $[Mn^{II}-Mn^{III}-Mn^{II}]$ complex and explaining the relatively high room-temperature χT value (vide supra). At lower temperatures (Figure 5), the χT product decreases likely due to the combined effect of weak intercomplex antiferromagnetic interactions mediated by short C−H⋯Br contacts and magnetic anisotropy brought by the Mn^{III} metal ions. On the basis of the crystal structure (vide supra), the magnetic properties of **1** have been modeled in a first approach using an isotropic Heisenberg Hamiltonian considering only the intra-$[Mn_3]$ magnetic interaction (J): $\hat{H} = -2J(\hat{S}_A\hat{S}_1 + \hat{S}_1\hat{S}_B)$ with $\hat{S}_A$ and $\hat{S}_B$ being the peripheral Mn^{II} spin operators (with $S_A = S_B = 5/2$) and $\hat{S}_1$ the central Mn^{III} spin operators (with $S_1 = 2$). Unfortunately, the deduced analytical expression of the low-field magnetic susceptibility (given in the Supporting Information) was able to reproduce the magnetic data only down to 40 K. Therefore, in order to model also the lower temperature data, intercomplex magnetic interactions, J', have been added in the frame of the mean field approximation (see Supporting Information).[16] The experimental data down to 1.8 K are extremely well fitted to this model with the following set of magnetic parameters: $J/k_B = +5.5(2)$ K, $zJ'/k_B = -0.044(5)$ K, and $g = 1.99(5)$ (Figure 5, blue solid line). It is worth mentioning that a model considering only the intra-complex magnetic interaction, J, and the Mn^{III} magnetic anisotropy, D (defined by the following anisotropy Hamiltonian, $\hat{H}_A = D\hat{S}^2_{1,z}$), was not able to reproduce the experimental data as well as the above model (with physically meaningful D values). As expected from the quality of the fit shown in Figure 5, a complete model considering the Mn^{III} magnetic anisotropy in addition to the intercomplex magnetic interactions leads to an overparametrization of the fitting procedure and multiple sets of magnetic parameters, which all indicate the dominant role of the intercomplex magnetic interactions. Nevertheless, these couplings (−0.044(5) K) are certainly overestimated by the above model as this value contains phenomenologically the intrisic Mn^{III} magnetic anisotropy. The ferromagnetic intra-complex magnetic interaction, estimated at +5.5(2) K, indicates that **1** possess an $S_T = 7$ ground state with an $S = 6$ first excited state lying at 22 K above in energy. This ground state is further confirmed by the field dependence of the magnetization below 8 K (inset in Figure 5 and Figure S1, Supporting Information) and its saturation above 6 T at 1.8 K around 14 μ_B.[17] Alternating current susceptibility measurements were performed below 15 K and show the complete absence of out-

phase signal (and thus single-molecule magnet behavior) above 1.8 K.

For the three one-dimensional coordination networks of $[Mn_3]$ complexes, Figure 6 shows the temperature dependence of the χT product at 1000 Oe. At 270 K, the value of the χT product is 12.7, 11.8, and 12.0 cm^3 K mol^{-1} for **2∞**, **3∞**, and **4∞**, respectively. Like for **1**, these values are slightly higher than the theoretical spin-only value per $[Mn^{III}Mn^{II}_2L_2X_4]^+$ complex due to the dominant intra-$[Mn_3]$ ferromagnetic interactions. These ferromagnetic interactions are clearly observed lowering the temperature, as the χT product increases up to 14.0, 12.5, and 12.8 cm^3 K mol^{-1} at 72, 96, and 90 K for **2∞**, **3∞**, and **4∞**, respectively. Below these temperatures, the decrease of the χT product highlights the presence of significantly strong antiferromagnetic interactions certainly mediated by the end-to-end bridging azido groups between Mn^{II} metal ions along the chains. While the χT product almost vanishes at low temperature for compounds **3∞** and **4∞** as expected for antiferromagnetically coupled spin chains, the χT product of **2∞** exhibits an upturn with a succession of a minimum at 5 K around 4.3 cm^3 K mol^{-1}, a maximum at 2.7 K around 7.4 cm^3 K mol^{-1}, and finally a 1.8 K value of 6.2 cm^3 K mol^{-1}. On the basis of the crystal structures (vide supra), the magnetic susceptibility of these one-dimensional compounds has been modeled using the following classical spin chain Hamiltonian: $\hat{H} = -2\sum_{i=1}^{N} J_1(\hat{S}_{A,i}\hat{S}_{1,i} + \hat{S}_{1,i}\hat{S}_{B,i}) + J_2(\hat{S}_{B,i}\hat{S}_{A,i+1})$ with J_1 and J_2 being the Mn^{II}–Mn^{III} magnetic interaction within the $[Mn_3]$ repeating motif and the Mn^{II}–Mn^{II} magnetic interaction through the end-to-end azido group. The work of Fisher[18] was extended in order to calculate the magnetic susceptibility of this chain system (see Supporting Information), and experimental data have been fitted down to 1.8 K for **3∞** and **4∞** and above 20 K for **2∞**. As shown in Figure 6, excellent fits of the data are obtained with $J_1/k_B = +5.9(2)$ K, $J_2/k_B = -3.0(1)$ K, and $g = 2.00(5)$ for **2∞**, $J_1/k_B = +5.9(2)$ K, $J_2/k_B = -4.1(1)$ K, and $g = 1.96(5)$ for **3∞**, and $J_1/k_B = +5.9(2)$ K, $J_2/k_B = -3.9(1)$ K, and $g = 1.97(5)$ for **4∞**. As expected, the $S_T = 7$ ground state of the $[Mn^{III}Mn^{II}_2L_2X_4]^+$ complex, induced by the ferromagnetic Mn^{II}–Mn^{III} interactions (J_1), is preserved in these three chains and moreover almost unaffected by the azido coordination or the different used halide anions and ligands. On the other hand, estimations of the antiferromagnetic Mn^{II}–Mn^{II} interactions (from −3 to −4.1 K) through the end–end azido groups are in excellent agreement with the previously reported values (from −1.5 to −8 K).[19] As already mentioned, the magnetic susceptibility for **3∞** and **4∞** follows very well, down to 1.8 K, the expected properties of spin chains, but in the case of **2∞**, a clear departure from the one-dimensional property is observed below 20 K. Therefore, ac susceptibility measurements were performed at low temperature to detect a possible magnetic phase transition in **2∞**. As shown in Figure 7, a narrow ac peak is observed on both in-phase and out-of-phase components of the ac susceptibility. The weak frequency dependence and sharpness of the ac signal indicate the presence of a long-rang three-dimensional magnetic order with a spontaneous magnetization as demonstrated by the nonzero out-of-phase ac susceptibility. The critical temperature of the magnetic order can be estimated at 3.4 K based on the appearance of the out-of-phase component. Additional dc magnetization measurements were performed to characterize this magnetic ordered ground state (Figures S2–S3, Supporting Information, and Figures 7 and 8). As expected, at lower temperatures than the out-of-phase ac
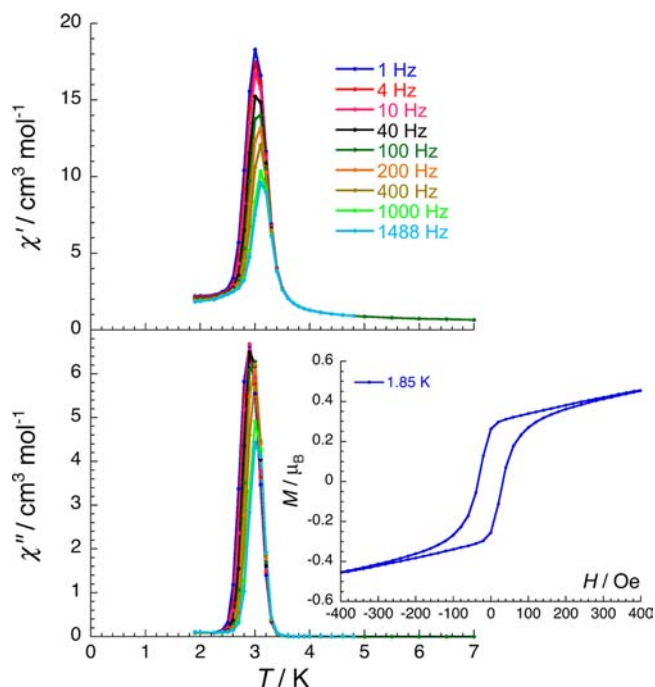

Figure 7. Temperature dependence of the real (χ', top) and imaginary (χ'', bottom) parts of the ac susceptibility at various ac frequencies between 1 and 1488 Hz for a polycrystalline sample of **2∞** in zero dc field. Solid lines are visual guides. (Inset) M vs H data at 35 Oe/min at 1.85 K for **2∞** illustrating the slow relaxation of the magnetization, i.e., the presence of a hysteresis effect. Solid line is a visual guide.
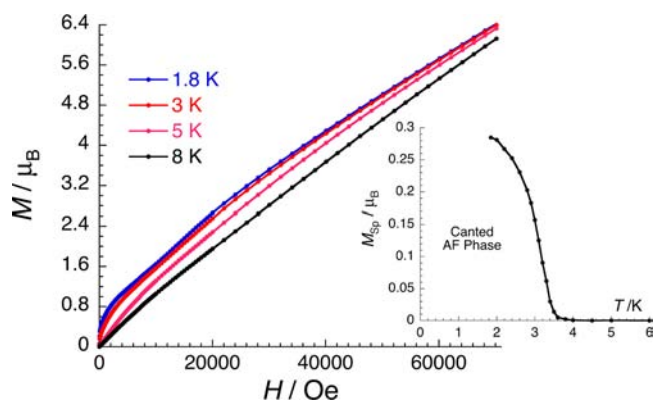

Figure 8. Field dependence of the magnetization for a polycrystalline sample of **2∞** between 1.8 and 6 K with sweep rates of 100–200 Oe/min. (Inset) Temperature dependence of the spontaneous magnetization for a polycrystalline sample of **2∞** between 1.8 and 6 K determined from Figure S3, Supporting Information.

peak (Figure 7) the magnetization at 1.8 K (inset Figure 7) exhibits a hysteresis effect (with a small coercive field of about 40 Oe), confirming the magnet behavior of **2∞**. Magnetization below 8 K (Figures 8 and S3, Supporting Information) rises very rapidly at low fields, below 100 Oe, and then increases linearly up to 7 T to reach 6.4 μ_B at 1.8 K, a value very far from the expected 14 μ_B for an $S = 7$ unit. This M vs H behavior is characteristic of a canted antiferromagnetic ground state possessing a small remnant or spontaneous magnetization resulting from the noncompensation of the two antiferromagnetically coupled magnetic sublattices. The temperature dependence of the spontaneous magnetization (inset of Figure 8) has been estimated from detailed low-field M vs H data

below 6 K (Figure S3, Supporting Information), confirming the critical temperature of 3.4 K. In the canted antiferromagnetic phase, the equilibrium canting angle, α, between the two magnetic sublattices is estimated at ca. 5° from the extrapolated 0 K value of the spontaneous magnetization, 0.3 μ_B (as $\sin(\alpha/2) = 2M_R/M_{sat}$, $M_{sat} \approx 14$ μ_B is the expected magnetization at saturation with $g = 2$).

On the basis of the above structural descriptions, the canted antiferromagnetic ground state of 2∞ is not a surprise considering that along the chain direction the local anisotropy axes (Jahn−Teller axis) of the Mn^{III} metal ions form an 84.8° angle between two neighboring $[Mn^{III}Mn^{II}_2(L_A)_2Br_4]^+$ units (Figure 2a). Moreover, the antiferromagnetically coupled chains are themselves not parallel in the crystal packing (Figure 2b), generating two different possible sources of spin canting in the materials. For 3∞, the absence of canting (Figure 6) is relatively straightforward to understand as the chains are arranged in a parallel fashion in the structure and along the chain; the Jahn−Teller axes are also all symmetrically aligned (Figure 3). Therefore, both intra- and interchain antiferromagnetic interactions can be satisfied in 3∞. As for 3∞, compound 4∞ does not show any sign of canting in its magnetic properties (Figure 6) even if the crystal structure reveals the presence of two chain orientations, while the Jahn−Teller axes along the chain are all parallel. This comparison suggests that the origin of the spin canting and thus the canted antiferromagnetic order in 2∞ is found in the nonparallel alignment of the Jahn−Teller axes along the chain.

CONCLUSIONS

In this work, we report the first three examples of covalently linked assemblies of $S_T = 7$ $[Mn^{III}Mn^{II}_2L_2X_4]^+$ cationic complexes using 1,3-diol-based ligands and azide bridging groups. By adjusting the steric hindrance of the pyridinium-functionalized 1,3-diol ligand, different chain organizations of this high-spin trinuclear manganese complex and different crystal packings of these one-dimensional azido-bridged coordination networks have been explored. While two of the compounds display the expected magnetic properties of spin chains with dominating antiferromagnetically coupling, the third compound is a magnet below 3.4 K. This magnet behavior, associated to a long-range canted antiferromagnetic order, results from the misalignment of the Jahn−Teller Mn^{III} axes along the chain and two chain orientations in the crystal structure. These results and the good stability of the $S_T = 7$ $[Mn^{III}Mn^{II}_2L_2X_4]^+$ cationic complexes prompts us to explore in the future other possible coordination networks of different dimensionalities using pyridinium-functionalized 1,3-diol ligands, other bridging groups, coordinating radicals, or metal complexes. These new systems could eventually stabilize effective ferromagnetic intercomplex interactions and thus new magnets at high temperatures.

ASSOCIATED CONTENT

ⓢ Supporting Information
Crystallographic tables and additional information; additional magnetic data; CIF files for the compounds. This material is available free of charge via the Internet at http://pubs.acs.org. CIF files can also be obtained free of charge from the Cambridge Crystallographic Data Centre with CCDC 833840, 834935, 855934, and 835269 (**1**, **2∞**, **3∞**, and **4∞**, respectively) via http://www.ccdc.cam.ac.uk/data_request/cif.

AUTHOR INFORMATION

Corresponding Author
*E-mail: wug@jlu.edu.cn (G.W.); sqiu@jlu.edu.cn (S.Q.); clerac@crpp-bordeaux.cnrs.fr (R.C.).

Notes
The authors declare no competing financial interest.

REFERENCES

(1) (a) Rüttinger, W.; Dismukes, G. C. *Chem. Rev.* **1997**, *97*, 1. (b) Rüttinger, W.; Yagi, M.; Wolf, K.; Bernasek, S.; Dismukes, G. C. *J. Am. Chem. Soc.* **2000**, *122*, 10353. (c) Law, N. A.; Caudle, M. T.; Pecoraro, V. L. *Adv. Inorg. Chem.* **1998**, 305. (d) Kostakis, G. E.; Ako, A. M.; Powell, A. K. *Chem. Soc. Rev.* **2010**, *39*, 2238. (e) Sartorel, A.; Bonchio, M.; Campagna, S.; Scandola, F. *Chem. Soc. Rev.* **2013**, *42*, 2262.

(2) (a) Sessoli, R.; Tsai, H.−L.; Schake, A. R.; Wang, S.; Vincent, J. B.; Folting, K.; Gatteschi, D.; Christou, G.; Hendrickson, D. N. *J. Am. Chem. Soc.* **1993**, *115*, 1804. (b) Sessoli, R.; Gatteschi, D.; Caneschi, A.; Novak, M. A. *Nature* **1993**, *365*, 141. (c) Thomas, L.; Lionti, F.; Ballou, R.; Gatteschi, D.; Sessoli, R.; Barbara, B. *Nature* **1996**, *383*, 145. (d) Clérac, R.; Miyasaka, H.; Yamashita, M.; Coulon, C. *J. Am. Chem. Soc.* **2002**, *124*, 12837. (e) Hill, S.; Edwards, E. S.; Aliaga-Alcalde, N.; Christou, G. *Science* **2003**, *302*, 1015.

(3) (a) Mishra, A.; Wernsdorfer, W.; Abboud, K. A.; Christou, G. *Chem. Commun.* **2005**, *1*, 54. (b) Hewitt, I. J.; Tang, J.; Madhu, N. T.; Clérac, R.; Buth, G.; Anson, C. E.; Powell, A. K. *Chem. Commun.* **2006**, 2650. (c) Barber, J.; Murray, J. W. *Coord. Chem. Rev.* **2008**, *252*, 233. (d) Koumousi, E. S.; Mukherjee, S.; Beavers, C. M.; Teat, S. J.; Christou, G.; Stamatatos, T. C. *Chem. Commun.* **2011**, *47*, 11128.

(4) (a) Christou, G.; Gatteschi, D.; Hendrickson, D. N.; Sessoli, R. *MRS Bull.* **2000**, *25*, 66. (b) Leuenberger, M.; Loss, D. *Nature* **2001**, *410*, 789. (c) Gatteschi, D.; Sessoli, R. *Angew. Chem., Int. Ed.* **2003**, *42*, 268. (d) Aromi, G.; Brechin, E. K. *Struct. Bonding (Berlin)* **2006**, *122*, 1. (e) Gatteschi, D.; Sessoli, R.; Villain, J. *Molecular Nanomagnets*; Oxford University Press: Oxford, 2006.

(5) (a) Wernsdorfer, W.; Aliaga-Alcalde, N.; Hendrickson, D. N.; Christou, G. *Nature* **2002**, *416*, 406. (b) Tiron, R.; Wernsdorfer, W.; Aliaga- Alcalde, N.; Christou, G. *Phys. Rev. B* **2003**, *68*, 140407(R). (c) Tiron, R.; Wernsdorfer, W.; Foguet-Albiol, D.; Aliaga-Alcalde, N.; Christou, G. *Phys. Rev. Lett.* **2003**, *91*, 227203.

(6) (a) Miyasaka, H.; Nakata, K.; Sugiura, K.; Yamashita, M.; Clérac, R. *Angew. Chem., Int. Ed.* **2004**, *43*, 707. (b) Yoo, J.; Wernsdorfer, W.; Yang, E.-C.; Nakano, M.; Rheingold, A. L.; Hendrickson, D. N. *Inorg. Chem.* **2005**, *44*, 3377. (c) Miyasaka, H.; Nakata, K.; Lecren, L.; Coulon, C.; Nakazawa, Y.; Fujisaki, T.; Sugiura, K.; Yamashita, M.; Clérac, R. *J. Am. Chem. Soc.* **2006**, *128*, 3770. (d) Andruh, M. *Chem. Commun.* **2007**, 2565. (e) Lecren, L.; Wernsdorfer, W.; Li, Y.-G.; Vindigni, A.; Miyasaka, H.; Clérac, R. *J. Am. Chem. Soc.* **2007**, *129*, 5045. (f) Xu, H.-B.; Wang, B.-W.; Pan, F.; Wang, Z.-M.; Gao, S. *Angew. Chem., Int. Ed.* **2007**, *46*, 7388. (g) Roubeau, O.; Clérac, R. *Eur. J. Inorg. Chem.* **2008**, 4325. (h) Bai, Y.-L.; Tao, J.; Wernsdorfer, W.; Sato, O.; Huang, R.-B.; Zheng, L.-S. *J. Am. Chem. Soc.* **2006**, *128*, 16428. (i) Liu, C.-M.; Zhang, D.-Q.; Zhu, D.-B. *Inorg. Chem.* **2009**, *48*, 4980. (j) Song, X.; Yang, P.; Mei, X.; Li, L.; Liao, D. *Eur. J. Inorg. Chem.* **2010**, 1689. (k) Jones, L. F.; Prescimone, A.; Evangelisti, M.; Brechin, E. K. *Chem Comm* **2009**, *15*, 2023. (l) Yang, C.-I.; Tsai, Y.-J.; Hung, S.-P.; Tsai, H.-L.; Nakano, M. *Chem. Commun.* **2010**, *46*, 5716.

(m) Moushi, E. E.; Stamatatos, T. C.; Wernsdorfer, W.; Nastopoulos, V.; Christou, G.; Tasiopoulos, A. J. *Inorg. Chem.* **2009**, *48*, 5049. (n) Lin, P.-H.; Burchell, T. J.; Clérac, R.; Murugesu, M. *Angew. Chem., Int. Ed.* **2008**, *47*, 8848. (o) Jeon, I.-R.; Clérac, R. *Dalton Trans.* **2012**, *41*, 9569.

(7) (a) Hill, C. L. *Chem. Rev.* **1998**, *98*, 1. (b) Pope, M. T.; Muller, A. *Polyoxometalate Chemistry from Topology via Self-Assembly to applications*; Kluwer Academic Publishers: The Netherlands, 2001. (c) Feng, P.; Bu, X.; Zheng, N. *Acc. Chem. Res.* **2005**, *38*, 293. (d) Dehnen, S.; Melullis, M. *Coord. Chem. Rev.* **2007**, *251*, 1259. (e) Osterloh, F. E. *Chem. Mater.* **2008**, *20*, 35. (f) Anson, C. E.; Eichohfer, A.; Issac, I.; Fenske, D.; Fuhr, O.; Sevillano, P.; Persau, C.; Stalke, D.; Zhang, J. *Angew. Chem., Int. Ed.* **2008**, *47*, 1326. (g) Long, D.; Tsunashima, R.; Cronin, L. *Angew. Chem., Int. Ed.* **2010**, *49*, 1736. (h) Vaqueiro, P. *Dalton Trans.* **2010**, *39*, 5965.

(8) (a) Yaghi, O. M.; Li, H.; Davis, C.; Richardson, D.; Groy, T. L. *Acc. Chem. Res.* **1998**, *31*, 474. (b) Eddaoudi, M.; Moler, D.; Li, H.; Reineke, T. M.; O'Keeffe, M. O.; Yaghi, M. *Acc. Chem. Res.* **2001**, *34*, 319. (c) Cotton, F. A.; Lin, C.; Murillo, C. A. *Acc. Chem. Res.* **2001**, *34*, 759. (d) Tranchemontagne, D. J.; Mendoza-Cortes, J. L.; O'Keeffe, M.; Yaghi, O. M. *Chem. Soc. Rev.* **2009**, *38*, 1257. (e) Perry, J. J., IV; Perman, J. A.; Zaworotko, M. J. *Chem. Soc. Rev.* **2009**, *38*, 1400. (f) Ferey, G.; Mellot-Draznieks, C.; Serre, C.; Millange, F.; Dutour, J.; Surble, S.; Margiolaki, I. *Science* **2005**, *309*, 5743. (g) Dinca, M.; Dailly, A.; Long, J. R. *Chem.—Eur. J.* **2008**, *14*, 10280.

(9) Rao, C. N. R.; Natarajan, S.; Choudhury, A.; Neeraj, S.; Ayi, A. A. *Acc. Chem. Res.* **2001**, *34*, 80 and references therein.

(10) (a) Milios, C. J.; Inglis, R.; Vinslava, A.; Bagai, R.; Wernsdorfer, W.; Parsons, S.; Perlepes, S. P.; Christou, G.; Brechin, E. K. *J. Am. Chem. Soc.* **2007**, *129*, 12505. (b) Milios, C. J.; Inglis, R.; Jones, L. F.; Prescimone, A.; Parsons, S.; Wernsdorfer, W.; Brechin, E. K. *Dalton Trans.* **2009**, *15*, 2812. (c) Jones, L. F.; Prescimone, A.; Evangelisti, M.; Brechin, E. K. *Chem. Commun.* **2009**, *15*, 2023. (d) Inglis, R.; Kastenis, A. D.; Collins, A.; White, F.; Milios, C. J.; Papaefstatiou, G. S.; Brechin, E. K. *CrystEngChem* **2010**, *12*, 2064. (e) Flamourakis, A. G.; Tzimopoulos, D.; Siczek, M.; Lis, T.; O'Brien, J. R.; Akrivos, P. D.; Milios, C. J. *Dalton Trans.* **2011**, *40*, 11371. (f) An, G.; Cui, A.; Kou, H. *Inorg. Chem. Commun.* **2011**, *14*, 1475.

(11) (a) Yoo, J.; Wernsdorfer, W.; Yang, E.; Nakano, M.; Rheingold, A. L.; Hendrickson, D. N. *Inorg. Chem.* **2005**, *44*, 3377. (b) Lecren, L.; Roubeau, O.; Coulon, C.; Li, Y.; Le Goff, X. F.; Wernsdorfer, W.; Miyasaka, H.; Clérac, R. *J. Am. Chem. Soc.* **2005**, *127*, 17353. (c) Miyasaka, H.; Nakata, K.; Lecren, L.; Coulon, C.; Nakazawa, Y.; Fujisaki, T.; Sugiura, K.; Yamashita, M.; Clérac, R. *J. Am. Chem. Soc.* **2006**, *128*, 3770. (d) Taguchi, T.; Daniels, M. R.; Abboud, K. A.; Christou, G. *Inorg. Chem.* **2009**, *48*, 9325. (e) Taguchi, T.; Wernsdorfer, W.; Abboud, K. A.; Christou, G. *Inorg. Chem.* **2010**, *49*, 199. (f) Taguchi, T.; Wernsdorfer, W.; Abboud, K. A.; Christou, G. *Inorg. Chem.* **2010**, *49*, 10579.

(12) (a) Moushi, E. E.; Stamatatos, T. C.; Wernsdorfer, W.; Nastopoulos, V.; Christou, G.; Tasiopoulos, A. J. *Angew. Chem., Int. Ed.* **2006**, *45*, 7722. (b) Moushi, E. E.; Lampropoulos, C.; Wernsdorfer, W.; Nastopoulos, V.; Christou, G.; Tasiopoulos, A. J. *Inorg. Chem.* **2007**, *46*, 3795. (c) Moushi, E. E.; Masello, A.; Wernsdorfer, W.; Nastopoulos, V.; Christou, G.; Tasiopoulos, A. J. *Dalton Trans.* **2010**, *39*, 4978. (d) Nayak, S.; Beltran, L. M. C.; Lan, Y.; Clérac, R.; Hearns, N. G. R.; Wernsdorfer, W.; Anson, C. E.; Powell, A. K. *Dalton Trans.* **2009**, 1901. (f) Moushi, E. E.; Lampropoulos, C.; Wernsdorfer, W.; Nastopoulos, V.; Christou, G.; Tasiopoulos, A. J. *J. Am. Chem. Soc.* **2010**, *132*, 16146. (g) Wu, G.; Huang, J.; Sun, L.; Bai, J.; Li, G.; Cremades, E.; Ruiz, E.; Clérac, R.; Qiu, S. *Inorg. Chem.* **2011**, *50*, 8580. (h) Charalambous, M.; Moushi, E. E.; Constantina Papatriantafyllopoulou, C.; Wernsdorfer, W.; Nastopoulos, V.; Christou, G.; Tasiopoulos, A. J. *Chem. Commun.* **2012**, *48*, 5410. (i) Moushi, E. E.; Stamatatos, T. C.; Nastopoulos, V.; Christou, G.; Tasiopoulos, A. J. *Polyhedron* **2009**, *28*, 1814.

(13) Sarac, A. S.; Ozgul, S. E.; Gencturk, A.; Schulz, B.; Gilsing, H.; Faltz, H. *Prog. Org. Coat.* **2010**, *69*, 527.

(14) (a) *Software packages SMART, and SAINT*; Siemens Analytical X-ray Instruments Inc.: Madison, WI, 1996. (b) Sheldrick, G. M. *SHELX-97. Programs for Crystal Structure Solution and Refinement*; University of Göttingen: Göttingen, Germany, 1997.

(15) (a) Yoshino, A.; Miyagi, T.; Asato, E.; Mikuriya, M.; Sakata, Y.; Sugiura, K.; Iwasaki, K.; Hino, S. *Chem. Commun.* **2000**, 1475. (b) Prescimone, A.; Wolowska, J.; Rajaraman, G.; Parsons, S.; Wernsdorfer, W.; Murugesu, M.; Christou, G.; Piligkos, S.; McInnes, E. J. L.; Brechin, E. K. *Dalton Trans.* **2007**, 5282. (c) Saha, A.; Abboud, K.; Christou, G. *Inorg. Chem.* **2011**, *50*, 12774.

(16) (a) O'Connor, C. J. *Prog. Inorg. Chem.* **1982**, *29*, 203. (b) Myers, B. E.; Berger, L.; Friedberg, S. *J. Appl. Phys.* **1969**, *40*, 1149.

(17) It is worth noting that the M vs H/T or M vs H data cannot be fitted properly to a simple $S_T = 7$ macrospin model due to the presence of significant antiferromagnetic clearly seen at low field at 1.8 K.

(18) Fisher, M. E. *Am. J. Phys.* **1964**, *32*, 343.

(19) (a) Escuer, A.; Vicente, R.; Goher, M. A. S.; Mautner, F. A. *Inorg. Chem.* **1996**, *35*, 6386. (b) Ribas, J.; Escuer, A.; Monfort, M.; Vicente, R.; Corté s, R.; Lezama, L.; Rojo, T. *Coord. Chem. Rev.* **1999**, *195*, 1027−1068. (c) Zeng, Y.-F.; Hu, X.; Liu, F.-C.; Bu, X.-H. *Chem. Soc. Rev.* **2009**, *38*, 469. (d) Ma, Y.; Cheng, A.; Sun, W.; Zhang, J.; Gao, E. *Inorg. Chem. Commun.* **2009**, *12*, 412.